iScience

CellPress
OPEN ACCESS

Article

Kirigami-inspired automatically self-inclining bifacial solar cell arrays to enhance energy yield under both sunny and cloudy conditions

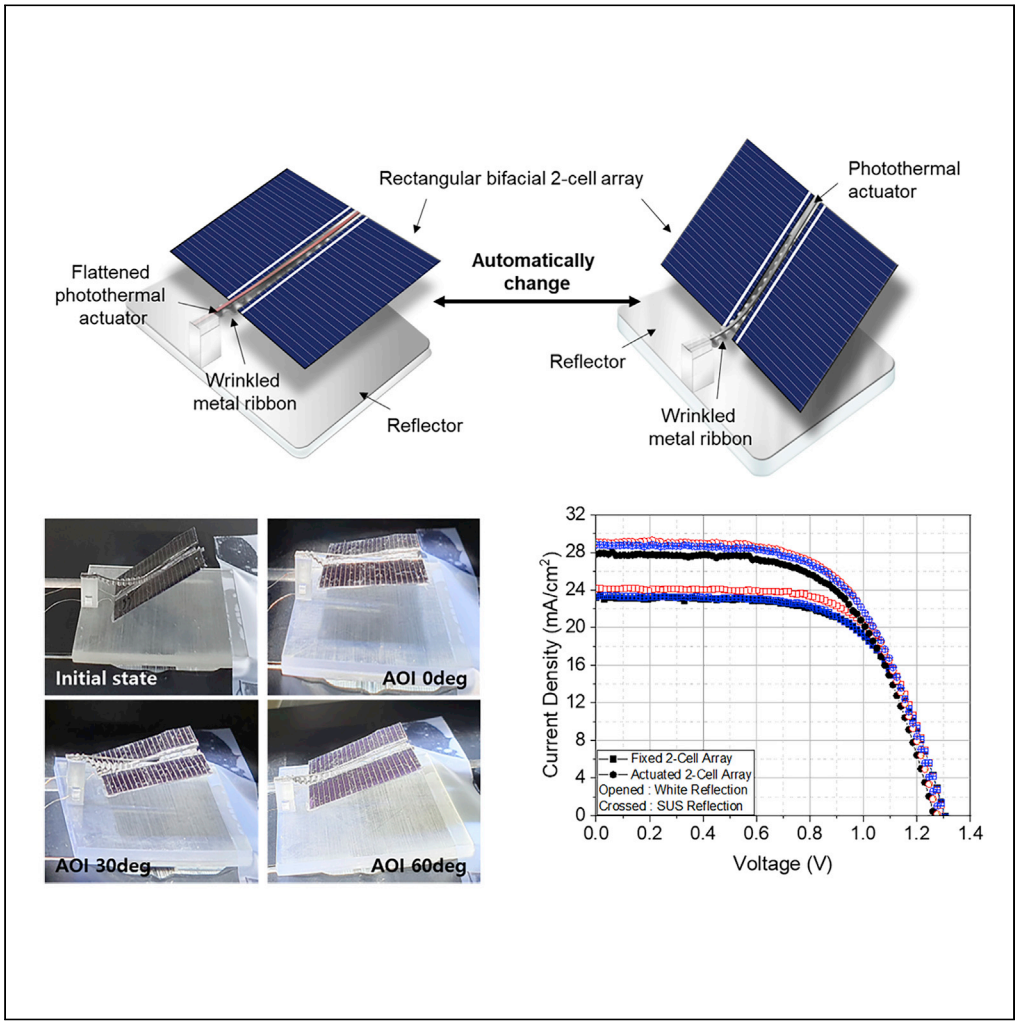

Min Ju Yun, Yeon Hyang Sim, Dong Yoon Lee, Seung I. Cha

sicha@keri.re.kr

Highlights

Proposing self-inclinable bifacial solar cell array depends on the weather condition

It can automatically change its alignment angle using a photothermal actuator

By self-incline at the appropriate angle, maximize captured light

It shows better performance under predominantly diffused incident light

Yun et al., iScience 25, 104649
July 15, 2022 © 2022 The Author(s).
https://doi.org/10.1016/j.isci.2022.104649

iScience

CellPress
OPEN ACCESS

Article

Kirigami-inspired automatically self-inclining bifacial solar cell arrays to enhance energy yield under both sunny and cloudy conditions

Min Ju Yun,[1] Yeon Hyang Sim,[1,2] Dong Yoon Lee,[1] and Seung I. Cha[1,2,3,*]

SUMMARY

The application of photovoltaics (PVs) is expanding in various locations ranging from industrial facilities to residential housing. The emphasized concept in the PVs field is shifting from "watt-per-cost" to "energy-yield-per-watt." To attain a high energy yield, fixed modules are not well suited to capture both direct and omnidirectional light. To achieve a high energy yield under both light conditions, we propose a self-inclining bifacial solar cell array fabricated by integrating a photothermal actuator, which senses incident light by itself, and actuating solar cells that incline at the appropriate angle to maximize captured light. In the vertical illumination state, the specific power of the self-inclining bifacial two-cell array is 11% higher than a fixed-angle aligned array. In an outside environment with a large proportion of diffused light, the self-inclining bifacial two-cell array also shows higher performance. We expect this work to enable PVs to be applied without regard to weather conditions.

INTRODUCTION

In response to environmental issues, the development of carbon-neutral cities and systems has become a worldwide priority (Garriga et al., 2020; Tozer and Klenk, 2018, 2018, 2018). Many researchers are, therefore, investigating methods to replace conventionally produced electricity with renewable energy. Among renewable energy systems, photovoltaics (PVs) are the most widely used, and PV energy is expected to be accountable for a large portion of consumed electricity in the future (Benda and Černá, 2020; Nam et al., 2020; Rabaia et al., 2021). Given this trend, the application of PVs has expanded in various geographical locations and in facilities ranging from industrial sites to residential housing. In addition, the emphasized concept in the PV field is shifting from "watt-per-cost" to "energy-yield-per-watt," especially for urban applications (Chen et al., 2021; Maghrabie et al., 2021; Seo et al., 2021; Sinke, 2019). Achieving a high energy yield in a solar plant requires a system with a tracking system and one-size-fits-all modules whose arrangement, including fixed angles and heights. In urban environments, solar plants are difficult to install; the module itself should, therefore, accommodate considerations beyond one-size-fits-all designs and strategies to achieve a high energy yield. Also, given the large proportion of diffused light in urban environments, a PV system should deliver optimal performance under both direct- and diffused light conditions.

To obtain high energy yield from PV systems in an urban environment, many researchers have proposed many solar cell technologies, including organic solar cells (Zhang et al., 2021; Liu et al., 2022) and at the same time, improved conventional silicon-based solar cells to bifacial structures to capture direct light, diffused light, and albedo reflected light. These technologies are based on the concept of a stand-alone bifacial module, an east–west-facing vertical module, and a module tilted at an optimized angle (Baumann et al., 2019; Jang and Lee, 2020; Nussbaumer et al., 2020; Patel et al., 2019, 2021; Raina et al., 2021). However, to attain maximum energy yield in a directly illuminated environment, a solar cell module should face the direction of incident light. In diffused-light environments such as shadows, a bifacial solar cell module should capture omnidirectional diffused light at both its front and back sides. Therefore, directly illuminated sunlight and diffused, scattered light require very different structures for their effective capture, and the incident light at a given point can change between direct and diffused light frequently and almost randomly, precluding an accurate prediction of the light conditions. Thus, the current typical fixed module structures cannot achieve optimal performance under these various incident light conditions.

[1]Energy Conversion Research Center, Electrical Materials Research Division, Korea Electrotechnology Research Institute, Changwon-si, Gyeongsangnam-do 51543, Korea

[2]Department of Electro-functionality Materials Engineering, University of Science and Technology, Changwon-si, Gyeongsangnam-do 51543, Korea

[3]Lead contact

*Correspondence: sicha@keri.re.kr

https://doi.org/10.1016/j.isci.2022.104649

This is an open access article under the CC BY-NC-ND license (http://creativecommons.org/licenses/by-nc-nd/4.0/).

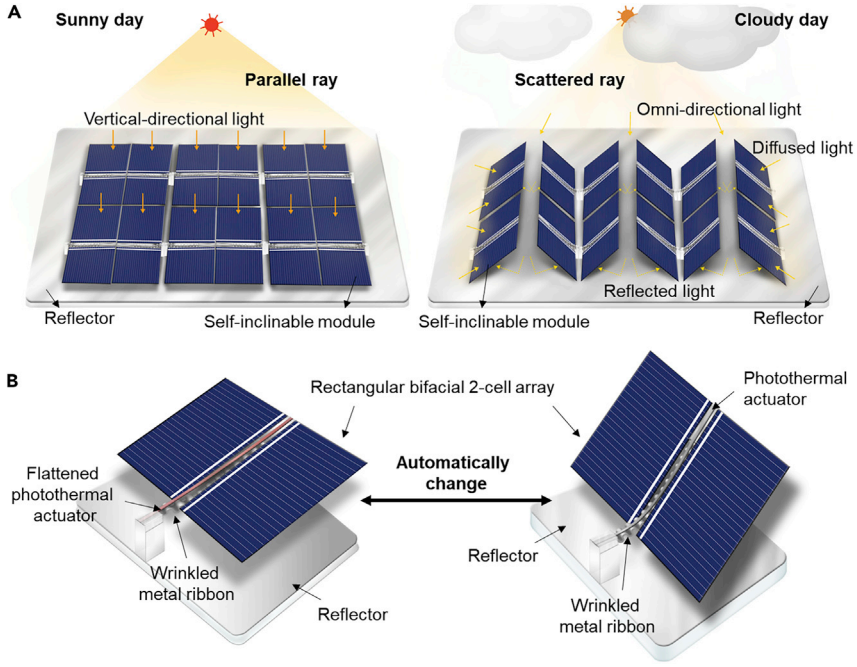

Figure 1. Main concept schematic of self-inclining bifacial solar cell array

(A and B) Schematics of (A) a self-inclining bifacial solar cell array under sunny and cloudy conditions and (B) the components of the self-inclining bifacial two-cell array that changes its alignment angle depending on the illumination environment.

To overcome this shortcoming, we here propose new solar-cell-array-based PV units that automatically change their facing angles according to the light condition via a photothermal actuator that senses the incident-light condition (i.e., direct sunlight or diffused light) by itself. The photothermal actuator actuates solar cells to achieve the appropriate angle of inclination: either a planar structure to capture direct and strong sunlight or an obliquely angled structure to capture diffused, omnidirectional light on both sides and on a reflector. In the vertical illumination state, the specific power of the self-inclining bifacial two-cell array is 11% greater than that of a fixed-angle aligned array, and the performance is enhanced by a reflector. We have confirmed the bifacial two-cell array's performance in an actual outside environment with a large proportion of diffused light. The self-inclining bifacial two-cell array also demonstrates better performance than a planar structure array such as a typical panel. Through this research, we expect to develop a bifacial solar cell that can function on either sunny or cloudy days or under conditions where the weather changes suddenly.

RESULTS

To achieve maximal energy gain in a module irrespective of sunny or cloudy conditions, we propose an automatically self-inclining bifacial solar cell array that can change its angle of inclination for parallel or scattered incident light, as shown in Figure 1A. Under direct and intense illumination conditions, the bifacial solar cell array automatically leans down, becoming planar with respect to parallel rays and receiving maximal incident light to produce maximal energy. When the environment is shadowed or under cloudy conditions, the array automatically inclines to assume a structure that favors the capture of omnidirectional scattered light, diffused light, and reflected light. The bifacial solar cell array can lean itself automatically because a photothermal actuator that assumes a memorized shape in response to a thermal stimulus is integrated into the array. The components required for the self-inclining bifacial solar cell array are shown in Figure 1B. For parallel rays (Figure 1B, left), the photothermal actuator's surface temperature is increased by incident light, leading to a change in shape to a memorized flattened shape through a phase-transition mechanism. Because of the actuator's change to a flat shape, the array also becomes planar with respect to rays from the vertical direction and automatically transforms into an optimized shape that can receive maximum parallel light. Under omnidirectional scattered rays, the photothermal actuator changes into

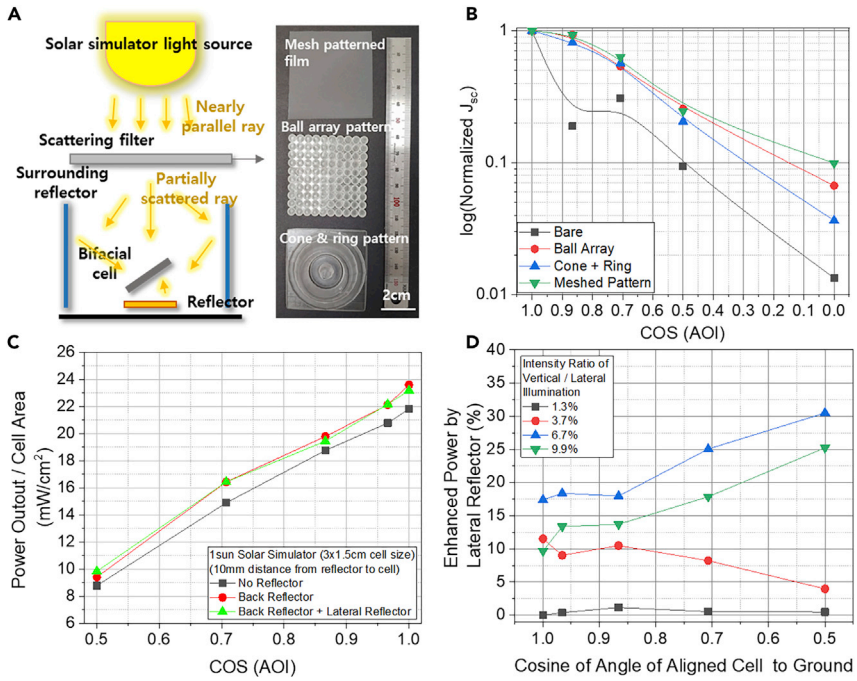

Figure 2. Bifacial solar cell's performance under scattered, diffused, and reflected illumination environments

(A) Schematic of scattered, diffused, and reflected illumination environments simulated using a patterned filter.

(B) Relationship between the normalized current density and the cosine of the angle of incidence for a bifacial solar cell in various scattered light environments controlled by a patterned filter.

(C) Effects of reflection and tilt on the bifacial solar cell's performance.

(D) Relationship between the enhanced power and alignment angle of the bifacial solar cell, which depends on vertical/lateral reflection ratio.

an elastic state because of the decreased heat; the array then automatically inclines as a result of the strong elasticity of a wrinkled metal ribbon on the back side of the photothermal actuator. Thus, the array has an optimized structure for capturing scattering, diffused, and reflected light on both sides of its bifacial solar cell. This device is proposed as a bifacial solar cell array that produces maximal power by changing its alignment angle automatically in response to the illumination environment (i.e., sunny or cloudy conditions).

The concepts proposed in Figure 1 to obtain maximal energy in both cases of direct illumination and scattered illumination conditions using bifacial solar cells are supported by the results of previous studies on monofacial solar cells and by the additional power gain of bifacial solar cells at various angles under different illumination conditions (Younas et al., 2019; Yun et al., 2020; Raina et al., 2021; Bernardi et al., 2012; Cui et al., 2019; Huang et al., 2020). These previously reported results—where the angled alignment of monofacial modules or arrays has been shown to affect the energy yield and where a vertical array of PV modules has been shown to produce more energy under scattered light conditions such as cloudy days by capturing other forms of incident light—have been expanded in the present work to a bifacial solar cell to confirm the effect of its angled alignment under a scattered- and diffused-light environment (Tayagaki and Yoshita, 2022; Yin et al., 2021).

To estimate the effect of omnidirectional light on the bifacial solar cells in a solar simulator, we used several light-scattering filters and surrounding reflectors to achieve several different illumination conditions (Figure 2A). We varied the scattering conditions using a mesh-patterned film, a ball-array-patterned plate, and a cone-and-ring-patterned plate; detailed photographs are shown in Figure S1. In the case of the mesh-patterned film, parallel rays were scattered by round metal wire and openings within the mesh patterns. In the case of the ball-array patterns, illuminated light was scattered through arranged 5 mm-diameter spheres. The cone-and-ring pattern that included a long cone with a diameter of 10 mm and a height of 10 mm was located in the center, and donut-ring shapes with various diameters and heights surrounded the cone, resulting in a scattering effect. In this case, the light cannot be regarded as fully omnidirectional

like a light in the external environment, which includes some proportion of diffused light; the effect of the light distribution performance on bifacial solar cells is, therefore, estimated. As shown in Figure 2B, the angled alignment effect is confirmed to be more substantial under omnidirectional illumination using scattering filters than under the unfiltered-light conditions, even though the light is artificial. We have also confirmed that the power production of a bifacial solar cell array underlying the reflector is enhanced in the parallel-ray illumination state and the power production is degraded according to the alignment angle Figure 2C). However, to estimate the effect of diffused and reflected light, we varied the vertical-to-lateral light intensity ratio from 1.3% to 9.9% via the reflector (Figure 2A), as shown in Figure 2D. This result confirms that the angled alignment of the bifacial cell enhances power production under omnidirectional diffused light. In an environment where the proportion of diffusion light is large, the power production increases with increasing angle of alignment, which is an important factor for the bifacial solar cell alignment array. Therefore, to obtain maximal energy under both direct- and diffused light conditions, the bifacial cells should be aligned differently according to the light conditions. Unfortunately, light conditions change unpredictably in the actual operating state; thus, self-sensing and actuation are required to respond to changes in actual light conditions.

To make the bifacial solar cell change automatically and align itself according to the light conditions, we integrated a shape memory alloy actuator that undergoes a phase transition to change to a memorized shape by sensing heat arising from photothermal transference from illuminated light and reflected light on an attached metal plate (Niu et al., 2022; Taya et al., 2013) as shown as Figure S2 and Video S1. A shape-memory alloy (SMA) was used as a photothermal actuator, and its transition temperature was measured through differential scanning calorimetry (DSC) analysis (Figure S3). The SMA's austenite start (A_s) temperature was 20.8°C, its austenite finishing (A_f) temperature was 31.2°C during heating, and its martensite start (M_s) temperature was 7.7°C during cooling. At temperatures less than the A_s temperature, the SMA shows elastic character; at temperatures greater than the A_s temperature, it becomes stiff and changes to its memorized shape. At temperatures greater than the A_f temperature, it completely transforms. We confirmed that the A_s temperature is rapidly reached, enabling the SMA to undergo a phase change under vertical illumination in conjunction with reflection and transmission of the metal material.

To incline the solar cell automatically at an angle, the wrinkled metal ribbon stands the solar cell upright via an elastic force. The elastic wrinkled metal ribbon was fabricated using an etched stainless steel (SUS) plate (Figure S4) with a thickness of 50.8 μm and 23% opening area; it was thus less stiff than a stainless steel plate and was imprinted with rolling pinion on a rack gear (Figure S5). Pressing force exerted during the rolling of the pinion rounded the metal ribbon, which has a semi-circle shape with a certain diameter (Figure 3A). The combination of the rounded wrinkled metal ribbon, which is elastic, and the SMA, which is superelastic, resulted in a balanced angle. A closing elastic force is exerted at each end of the combined actuator, which makes the balanced angle small via the metal ribbon; the reverse opening force is exerted through the SMA, which transforms to a memorized flattened shape via the photothermal effect. Because of the wrinkled metal ribbon's wavy structure, a weakly deformed zone and a heavily deformed zone with a smaller radius are attached to the SMA's surface. In the heavily deformed zone, illuminated light is reflected by the surface of the ribbon within the bay region and transfers photothermal energy to the attached SMA. Upon shape transformation of the SMA, the weakly deformed zone expands elastically. To confirm the deformation and recovery behavior of the combined rounded wrinkled metal ribbon and SMA, we first induced artificial heating using a convection oven (70°C). The combined wrinkled metal ribbon/SMA deformed by sensing the radiated heat; its opening force resulted in a maximized balanced angle. After deformation, we confirmed the automatic recovery function by allowing the combined metal ribbon/SMA with a maximized balanced angle to stand at room temperature, which resulted in a closing force. In addition, maintenance of the initial elastic state was confirmed even after repeated deformation of the maximized balanced angle through the heat-sensing/recovery behavior. After five repeated deformations, the combined metal ribbon/SMA recovered to the same balanced angle; thus, it maintained the elastic force of the wrinkled metal ribbon as the initial state (Figure 3B). Also, when the metal ribbon width was small, the maximized balanced angle achieved by the opening force generated by the SMA was the same as when the metal ribbon width was larger. However, the recovered balanced angle was smaller according to smaller width of wrinkled metal ribbon because the stronger the force of larger metal ribbon, the closing force was greatly generated. Through these results, it is confirmed that combined wrinkled metal ribbon/SMA can be deformed by opening force of SMA under illumination state and recovered to initial state by closing elastic force of wrinkled metal ribbon.

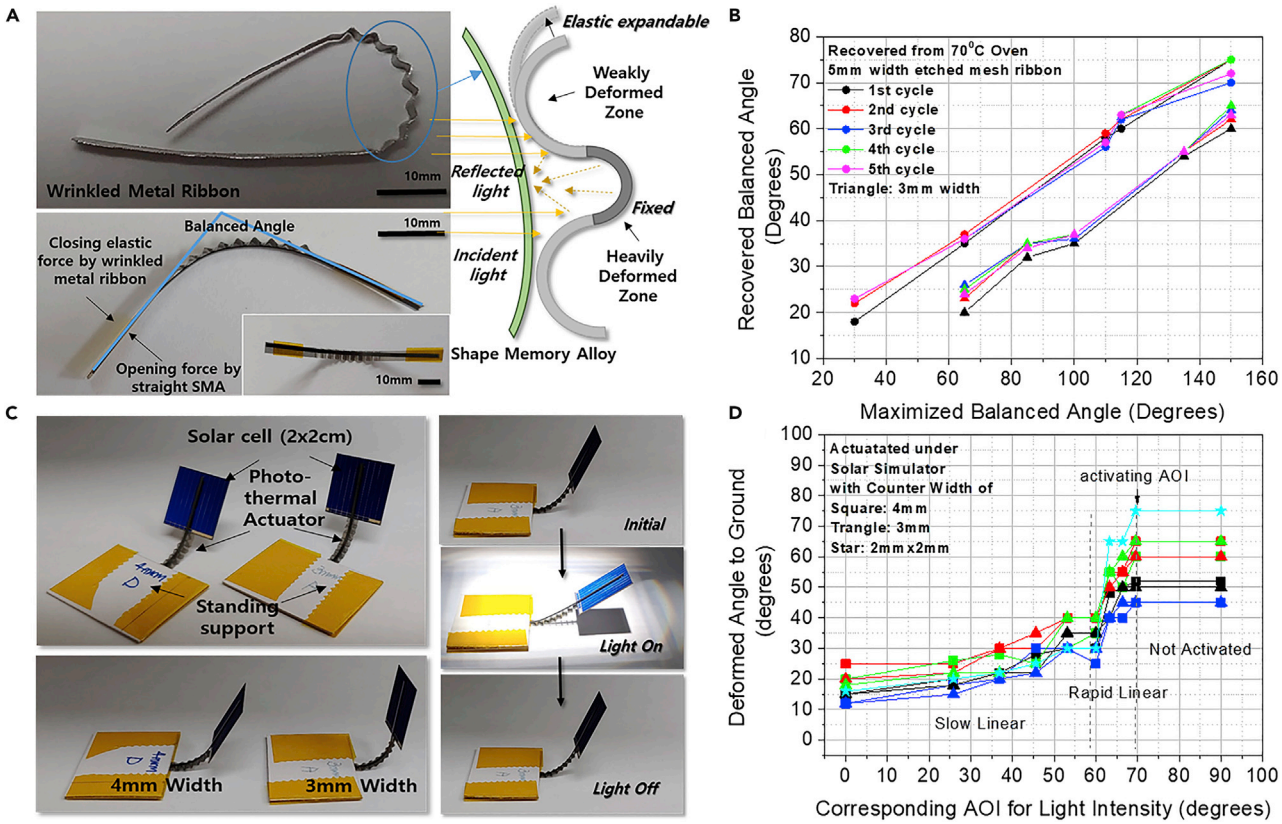

Figure 3. Performance of photothermal actuator

(A) Photograph of a wrinkled metal ribbon (top) and the formed balanced angle with closing elastic force and opening force generated by the combined wrinkled metal ribbon/SMA device (bottom). Schematic of the deformation behavior according to the shape change of the SMA.

(B and C) Cycle test of maximal opening and recovery of the combined wrinkled metal ribbon/SMA device. Photograph of (c) the self-inclining solar cell with an integrated SMA, wrinkled metal ribbon, and standing support (left top).

(D) The difference in alignment angle depending on the width of the metal ribbon (left bottom), and the self-inclining and recovery behavior under one Sun illumination and under the dark state. (D) Relationship between the deformation angle and the angle of incidence of the self-inclining solar cell according to the width of the metal ribbon.

We integrated the combined photothermal actuator/wrinkled metal ribbon into a solar cell and standing support and confirmed actuation under simulated sunlight (Figure 3C). We thus confirmed that the balanced angle was smaller when the width of the metal ribbon was narrower (Figure 3C, bottom). Under vertical directional illumination, the bifacial solar cell with an integrated combined wrinkled metal ribbon/SMA achieved an almost lying-down state with a large balanced angle as a result of the opening force; under the dark state, the bifacial solar cell inclined and recovered its initial balanced angle state as a result of the closing elastic force. To estimate the alignment angle of the solar cell according to the illumination conditions, we measured the deformation angle with respect to the ground (the deformation angle indicated in Figure S6) in devices with wrinkled metal ribbons with various widths (Figure 3D). Until the angle of incidence (AOI) reached 40°, the deformed angle ranged from 10° to 30° by the increased surface temperature of combined wrinkled metal ribbon/SMA above 32 degrees is over than SMA's A_f temperature and the solar cell, therefore, remained almost planar with respect to the incident rays, enabling it to capture maximal incident light. At high AOIs, the bifacial solar cell automatically recovered by self-inclination with a high deformation angle with respect to the ground to receive diffused, scattered, and reflected light on both sides of the solar cell by inclining at high speed. This phenomenon is because the surface temperature of the combined wrinkled metal ribbon/SMA became lower than the A_f temperature.

By integrating a bifacial solar cell, photothermal actuator, wrinkled metal ribbon, and standing support, we fabricated a self-inclining solar cell array that achieves an optimal alignment angle under sunny, cloudy, shaded, or other illumination conditions and confirmed that the array undergoes a rapid automatic

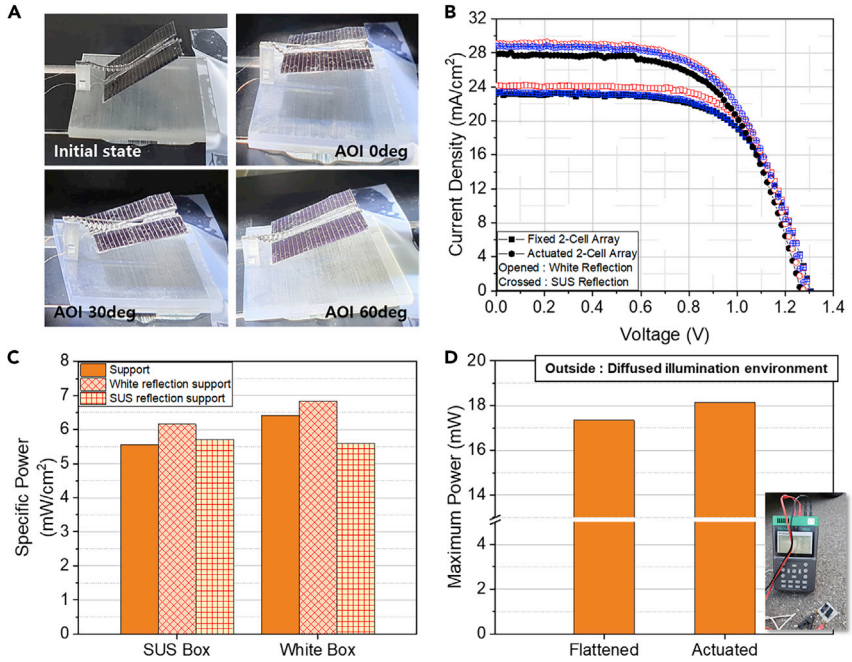

Figure 4. Photovoltaic performance of the self-inclining bifacial two-cell array

(A) Photograph of the self-inclining bifacial two-cell array under various light-illumination states ranging from direct and intense illumination to omnidirectional and diffused illumination.

(B) Photovoltaic performance of the self-inclining bifacial two-cell array and a fixed-angle bifacial two-cell array under one Sun illumination.

(C) The specific power depends on the box material used for artificial diffused light.

(D) Maximum power value of the flattened and self-inclinable bifacial two-cell array under outdoor conditions with predominantly diffused incident light.

transformation. Self-inclining solar cell array can be transformed within 20 s including sensing intensity of incident light. We estimated the PV performance of a two-cell bifacial array with a series-connected integrating actuator and a wrinkled metal ribbon. Under direct or intense illumination, the solar cell array leans down automatically and the alignment angle is small, almost planar with respect to the ray direction (Video S2). Under omnidirectional illumination, it automatically inclines with a high alignment angle to capture various forms of incident light. Under the dark state, it recovers to its initial state (Figure 4A). Under vertical directional illumination, the bifacial two-cell array with an integrated photothermal actuator demonstrated a specific power of 21.5 mW/cm^2, which is 11% greater than that of the fixed array (19.3 mW/cm^2) with the same alignment angle (40°), as shown in Figure S7. In addition, the specific power was increased by almost 6% by simply incorporating a white reflection plate as shown in Figure 4B and average value of three samples with the same condition to present detailed parameters of PV performance in Table S1. To estimate the performance of the bifacial two-cell array under omnidirectional illumination, we generated scattered rays from a solar simulator by using a mesh-patterned film and generated diffused rays using a box fabricated from SUS plates or white plates (Figure S8). The vertical-to-lateral light intensity ratio differed depending on the box material. In the case of the SUS and white boxes, the ratio was 3.4 and 15.6%, respectively; thus, within the white box, incident light was more reflected and diffused. In environments where the proportion of diffused light is much greater, PV performance is enhanced, as shown by the inclined arrangement in Figure 4C. PV performance can be further improved by replacing the standing support plate with a reflector SUS plate or white plate to reflect more light to the back side of the array. We estimated the bifacial two-cell array's performance in the actual outside environment. A similar illumination intensity was observed in measurements conducted with the solar array facing west, south, east, north, and skyward (bottom); thus, diffused incident light appears to be equally dispersed around the self-inclining bifacial two-cell array (Figure S9). The produced power was very small because of the low intensity of incident light; however, the PV performance of the integrated photothermal actuator was better than that of the planar structure similar to typical panels used in the outdoor environment (Figure 4D).

We have fabricated a self-inclining bifacial solar cell array by integrating a photothermal actuator that senses the light conditions and then automatically actuates them to achieve the proper angled arrangement. Self-actuation into an optimized structure was inspired by kirigami structures, and we have confirmed enhanced power production under both vertical-directional (sunny day) and omnidirectional and diffused (cloudy day) incident light by self-inclination to achieve either a planar structure or an angled alignment. This research will lead to a cornerstone power generation device that effectively utilizes a bifacial solar cell under any illumination environment, obviating the need to consider the intensity of incident light, shading, or sudden changes in the lighting conditions. We expect that this research will also contribute to the technical development of bifacial solar cell modules.

DISCUSSION

A self-inclinable bifacial solar cell array that can produce maximal energy under sunny, cloudy, or extreme weather conditions by automatically changing its alignment angle was proposed. To make the solar cell array incline itself, we combined an SMA as a photothermal actuator and a wrinkled metal ribbon. The combined device was then integrated into a bifacial solar array and standing support. Under direct and intense illumination, the photothermal actuator changed to a memorized flattened shape via transferred heat. The bifacial solar cell array changed to a planar configuration under direct illumination according to the change of the photothermal actuator. In reverse, under omnidirectional scattered and diffused illumination, the photothermal actuator changed to its elastic state and the wrinkled metal ribbon's elasticity force increased; thus, the bifacial solar cell array self-inclined. Under vertical illumination, the specific power of the self-inclinable bifacial two-cell array was 11% higher than that of a fixed tilted module; it also demonstrated better performance in the outdoor environment with predominantly diffused incident light. We expect the results of this research to lead to further development of bifacial solar cell technology and to enable the production of energy under any illumination conditions irrespective of the intensity of incident light, shading, or sudden external changes in illumination.

Limitations of the study

Suggested self-inclinable bifacial solar cell array showed better performance in the outdoor condition and from these results, it was emphasized that a PV module should be developed and utilized under all kinds of various incident lights like directional and omnidirectional like scattered, diffused, and reflected incident light. In this study, a simple 2-cell array that automatically changes according to the amount of light to maximize power was introduced. Expand from bifacial 2-cell array with these simple presentations and results to module scale, we should confirm the energy yield per day in the real environment.

Experimental procedures

Fabrication self-inclinable bifacial solar cell array

For the bifacial solar cell array, bifacial passivated emitter rear cells (Bifacial-PERC; LWM5BB-Bi-Fi-SE-223, Lightway) were used after being cut into rectangular shapes (15 × 30 mm, $w \times h$) using a fiber laser cutting system. Two bifacial solar cells were connected in series using a ribbon; this ribbon was also used to fix the two cells. Wires (commercial Cu wire (100 μm)) were then connected to each positive and negative electrode of the solar cell. Connections were soldered using Pb-free solder wire (HSE-02-SR34, Heesung Material) and a soldering iron (FX-951, Hakko). After the electrical connection of the array, the two cells were encapsulated via a casting process using silicone (polydimethylsiloxane (PDMS), Sylgard 184 A/B, Heesung STS) and then cured in a convection oven at 70°C. For the photothermal actuator, SMA components (Nitinol flat wires, Kellogg's Research Labs) with a flattened memorized shape were attached to the surface of the wrinkled metal ribbon. Metal ribbon (etched mesh) was imprinted with a wrinkled structure using a pinion-and-rack gear that we fabricated using a 3D printer (MonoX, Anycubic). The photothermal actuator and two-cell array were integrated into standing support that was also fabricated using a 3D printer; they were attached to the support using an adhesive (Loctite 401). The self-inclinable bifacial solar cell array maintained a 40° angled alignment naturally.

For the fixed two-cell array, an electrically connected and encapsulated solar cell array was attached to a tilted fixed frame fabricated using a 3D printer.

For the reflector plates, commercial stainless steel plates with high reflection and white plate fabricated with a 3D printer were used. To artificially diffuse light, we used boxes made of the SUS plate or white plate.

Characterization

DSC analysis (Q600, TA Instruments) was conducted from 0°C to 100°C at a heating/cooling rate of 10°C/min with the sample under a N_2 atmosphere to characterize the thermal properties of the SMA. For the measurement of the photovoltaic performance, we first calibrated a solar simulator (Sun, 2000, 1000 W Xe source; Abet Technologies; 2400 Keithley source meter) using a KG-3 filter and a reference cell certified by the National Renewable Energy Laboratory; the simulator was set to one Sun, 1.5 a.m.

STAR★METHODS

Detailed methods are provided in the online version of this paper and include the following:

- KEY RESOURCES TABLE
- RESOURCE AVAILABILITY
  - Lead contact
  - Materials availability

SUPPLEMENTAL INFORMATION

Supplemental information can be found online at https://doi.org/10.1016/j.isci.2022.104649.

ACKNOWLEDGMENT

This research was supported by the Korea Electrotechnology Research Institute (KERI) Primary Research Program through the National Research Council of Science & Technology (NST) funded by the Ministry of Science and ICT (MSIT) (No. 22A01005).

AUTHOR CONTRIBUTIONS

M.J.Y. and S.I.C. suggested an automatically self-inclining bifacial solar cell array concept and conducted experimental details and wrote the draft article and reviewed it. Y. H. S. contributed to detailed experiments for the encapsulation process and conformed power production under various incident light environments. D. Y. L. contributed to analyze the photothermal actuator's characteristics and gave feedback on the integration actuator and a wrinkled metal ribbon. All authors have reviewed the article and agreed regarding its submission.

DECLARATION OF INTERESTS

The authors declare no competing interests.

Received: April 4, 2022
Revised: May 31, 2022
Accepted: June 14, 2022
Published: July 15, 2022

REFERENCES

Baumann, T., Nussbaumer, H., Klenk, M., Dreisiebner, A., Carigiet, F., and Baumgartner, F. (2019). Photovoltaic systems with vertically mounted bifacial PV modules in combination with green roofs. Sol. Energy *190*, 139–146. https://doi.org/10.1016/j.solener.2019.08.014.

Benda, V., and Černá, L. (2020). PV cells and modules–State of the art, limits and trends. Heliyon *6*, e05666. https://doi.org/10.1016/j.heliyon.2020.e05666.

Bernardi, M., Ferralis, N., Wan, J.H., Villalon, R., and Grossman, J.C. (2012). Solar energy generation in three dimensions. Energy Environ. Sci. *5*, 6880. https://doi.org/10.1039/C2EE21170J.

Chen, C., Pinar, M., and Stengos, T. (2021). Determinants of renewable energy consumption: Importance of democratic institutions. Renew. Energy *179*, 75–83. https://doi.org/10.1016/j.renene.2021.07.030.

Cui, Y., Zhu, J., Zoras, S., Chen, X., Bi, H., Qiao, Y., and Soleimani, Z. (2019). State-of-the-art review of 3DPV technology: structures and models. Energy Convers. Manag. *200*, 112130. https://doi.org/10.1016/j.enconman.2019.112130.

Garriga, S.M., Dabbagh, M., and Krarti, M. (2020). Optimal carbon-neutral retrofit of residential communities in Barcelona, Spain. Energy Build. *208*, 109651. https://doi.org/10.1016/j.enbuild.2019.109651.

Huang, Y., Shigenobu, R., Yona, A., Mandal, P., Yan, Z., and Senjyu, T. (2020). M-shape PV arrangement for improving solar power generation efficiency. Appl. Sci. *10*, 537. https://doi.org/10.3390/app10020537.

Jang, J., and Lee, K. (2020). Practical performance analysis of a bifacial PV module and system. Energies *13*, 4389. https://doi.org/10.3390/en13174389.

Liu, J., Yin, Y., Wang, K., Wei, P., Lu, H., Song, C., Liang, Q., and Huang, W. (2022). Domain size control in all-polymer solar cells. iScience *25*, 104090. https://doi.org/10.1016/j.isci.2022.104090.

Maghrabie, H.M., Abdelkareem, M.A., Al-Alami, A.H., Ramadan, M., Mushtaha, E., Wilberforce, T., and Olabi, A.G. (2021). State-of-the-art technologies for building-integrated photovoltaic systems. Buildings *11*, 383. https://doi.org/10.3390/buildings11090383.

Nam, K., Hwangbo, S., and Yoo, C. (2020). A deep learning-based forecasting model for renewable energy scenarios to guide sustainable energy policy: a case study of Korea. Renew. Sustain. Energy Rev. *122*, 109725. https://doi.org/10.1016/j.rser.2020.109725.

Niu, D., Li, D., Chen, J., Zhang, M., Lei, B., Jiang, W., Chen, J., and Liu, H. (2022). SMA-based soft actuators with electrically responsive and photoresponsive deformations applied in soft robots. Sens. Actuator A Phys. *341*, 113516. https://doi.org/10.1016/j.sna.2022.113516.

Nussbaumer, H., Janssen, G., Berrian, D., Wittmer, B., Klenk, M., Baumann, T., Baumgartner, F., Morf, M., Burgers, A., Libal, J., and Mermoud, A. (2020). Accuracy of simulated data for bifacial systems with varying tilt angles and share of diffuse radiation. Sol. Energy *197*, 6–21. https://doi.org/10.1016/j.solener.2019.12.071.

Patel, M.T., Khan, M.R., Sun, X., and Alam, M.A. (2019). A worldwide cost-based design and optimization of tilted bifacial solar farms. Appl. Energy *247*, 467–479. https://doi.org/10.1016/j.apenergy.2019.03.150.

Patel, M.T., Ahmed, M.S., Imran, H., Butt, N.Z., Khan, M.R., and Alam, M.A. (2021). Global analysis of next-generation utility-scale PV: tracking bifacial solar farms. Appl. Energy *290*, 116478. https://doi.org/10.1016/j.apenergy.2021.116478.

Rabaia, M.K.H., Abdelkareem, M.A., Sayed, E.T., Elsaid, K., Chae, K.J., Wilberforce, T., and Olabi, A. (2021). Environmental impacts of solar energy systems: a review. Sci. Total Environ. *754*, 141989. https://doi.org/10.1016/j.scitotenv.2020.141989.

Raina, G., Vijay, R., and Sinha, S. (2021). Study on the optimum orientation of bifacial photovoltaic module. Int. J. Energy Res. *46*, 4247–4266. https://doi.org/10.1002/er.7423.

Seo, B., Kim, J.Y., and Chung, J. (2021). Overview of global status and challenges for end-of-life crystalline silicon photovoltaic panels: a focus on environmental impacts. Waste Manage. (Tucson, Ariz.) *128*, 45–54. https://doi.org/10.1016/j.wasman.2021.04.045.

Sinke, W.C. (2019). Development of photovoltaic technologies for global impact. Renew. Energy *138*, 911–914. https://doi.org/10.1016/j.renene.2019.02.030.

Taya, M., Liang, Y., Namli, O.C., Tamagawa, H., and Howie, T. (2013). Design of two-way reversible bending actuator based on a shape memory alloy/shape memory polymer composite. Smart Mater. Struct. *22*, 105003. https://doi.org/10.1088/0964-1726/22/10/105003.

Tayagaki, T., and Yoshita, M. (2022). Simulation of diffuse Irradiance impact on energy yield of curved photovoltaic modules using climatic datasets. IEEE J. Photovoltaics *12*, 526–532. https://doi.org/10.1109/JPHOTOV.2022.3143496.

Tozer, L., and Klenk, N. (2018). Discourses of carbon neutrality and imaginaries of urban futures. Energy Res. Soc. Sci. *35*, 174A–181. https://doi.org/10.1016/j.erss.2017.10.017.

Yin, H.P., Zhou, Y.F., Sun, S.L., Tang, W.S., Shan, W., Shen, X.D., and Shen, X. (2021). Optical enhanced effects on the electrical performance and energy yield of bifacial PV modules. Sol. Energy *217*, 245–252. https://doi.org/10.1016/j.solener.2021.02.004.

Patel, M.T., Khan, M.R., Sun, X., and Alam, M.A. (2019). Module technology for agrivoltaics: vertical bifacial versus tilted monofacial farms. IEEE J. Photovoltaics *247*, 467–479. https://doi.org/10.1016/j.apenergy.2019.03.150.

Yun, M.J., Sim, Y.H., Cha, S.I., and Lee, D.Y. (2020). Finding 10% hidden electricity in crystalline Si solar cells using PDMS coating and three-dimensional cell arrays. Prog. Photovoltaics Res. Appl. *28*, 372–381. https://doi.org/10.1002/pip.3246.

Zhang, Y., Wang, N., Wang, Y., Zhang, J., Liu, J., and Wang, L. (2021). All-polymer indoor photovoltaic modules. iScience *24*, 103104. https://doi.org/10.1016/j.isci.2021.103104.

STAR★METHODS

KEY RESOURCES TABLE

REAGENT or RESOURCE	SOURCE	IDENTIFIER
Chemicals, peptides, and recombinant proteins		
SYLGARD(R) 184 SILICONE ELASTOMER KIT		
Xylene	Heesung STS	1330-20-7
Ethylbenzene	Heesung STS	100-41-4
Dimethyl Siloxane, Dimethylvinylsiloxyterminated	Heesung STS	68083-19-2
Dimethylvinylated and trimethylated silica	Heesung STS	68988-89-6
Software and algorithms		
OriginPro 2019	Origin Lab	http://originlab.com
Other		
Shape Memory Alloy	Kellogg's Research Labs	NiTi Flat wire 0.6mm width
MonoX 3D printer	Anycubic	N/A
Eco UV resin		
Polyurethane acrylate		82116-59-4
Acrylate Monomer		29590-42-9
Photoinitiator		N/A

RESOURCE AVAILABILITY

Lead contact

Further information and requests for resources, measurement procedures and data can be directed to the lead contact, Dr. Seung I. Cha (sicha@keri.re.kr).

Materials availability

All solar cells, materials and chemicals could be available commercially.

Data and code availability

- All data reported in this paper will be shared by the lead contact upon request.
- There is no original code associated with this work.
- Any additional information required to reanalyze the data reported in this paper is available from the lead contact upon request.